Mechanism and Machine Theory 152 (2020) 103931

Contents lists available at ScienceDirect

Mechanism and Machine Theory

journal homepage: www.elsevier.com/locate/mechmachtheory

High-order based revelation of bifurcation of novel Schatz-inspired metamorphic mechanisms using screw theory

Xi Kang[a], Huijuan Feng[b], Jian S Dai[c,d], Haoyong Yu[a,*]

[a] Department of Biomedical Engineering, National University of Singapore, Singapore 117583, Singapore
[b] Reconfigurable Robotics Lab, École Polytechnique Fédérale de Lausanne (EPFL), 1015 Lausanne, Switzerland
[c] MOE Key Laboratory for Mechanism Theory and Equipment Design, Tianjin University, Tianjin 300350, China
[d] Advanced Kinematics and Reconfigurable Robotics Lab, School of Natural and Mathematical Sciences, King's College London, Strand, London WC2R 2LS, United Kingdom

ARTICLE INFO

Article history:
Received 9 February 2020
Revised 10 April 2020
Accepted 21 April 2020
Available online 7 June 2020

Keywords:
Metamorphic mechanism
Bifurcation
High-order kinematics
Screw theory

ABSTRACT

The revelation of mechanism bifurcation is essential in the design and analysis of reconfigurable mechanisms. The first- and second-order based methods have successfully revealed the bifurcation of mechanisms. However, they fail in the novel Schatz-inspired metamorphic mechanisms presented in this paper. Here, we present the third- and fourth-order based method for their bifurcation revelation using screw theory. Based on the constraint equations derived from the first- and second-order kinematics, only one linearly independent relationship between joint angular velocities at the singular configuration of the new mechanism can be generated, which means the bifurcation cannot be revealed in this way. Therefore, we calculate constraint equations from the third- and fourth-order kinematics, and attain two linearly independent relationships between joint angular accelerations at the same singular configuration that correspond to different curvatures of the kinematic curves of two motion branches in the configuration space. Moreover, motion branches in Schatz-inspired metamorphic mechanisms are demonstrated.

1. Introduction

Compared with traditional mechanisms with fixed mobility, reconfigurable mechanisms have variable numbers and types of mobility and a variety of configurations, which can meet the requirements for multi-tasks, multi-working conditions and multi-functions. The research of reconfigurable mechanism can be traced back to the 1990s. In 1996, Wohlhart discovered a kind of mechanism whose mobility would change when passing through a singular configuration and named it kinematotropic mechanism [1]. Later, Dai and Rees Jones proposed metamorphic mechanisms [2] based on the principle of biological evolution in the research of packaging origami decorations. These two kinds of mechanisms are the only two reconfigurable mechanisms developed in the 1990s, which extend traditional mechanisms to more broad wide application fields.

In the past 20 years, the bifurcation phenomenon of reconfigurable mechanisms has attracted many scholars' interest. Here, bifurcation (or multi-furcation) refers to the phenomenon that the mechanism has two (or more than two) different

* Corresponding author.
E-mail addresses: xi.kang@nus.edu.sg (X. Kang), huijuan.feng@epfl.ch (H. Feng), jian.dai@kcl.ac.uk (J.S. Dai), bieyhy@nus.edu.sg (H. Yu).

https://doi.org/10.1016/j.mechmachtheory.2020.103931

motion branches when it moves through a constrained singular configuration [3,4]. The revelation of bifurcation (or multi-furcation) is to detect whether there exist two (or more than two) different motion branches in a reconfigurable mechanism.

Some scholars found different motion branches of the mechanism by solving analytical solutions of the closed-loop equation based on the DH transformation matrix. Feng et al. [5,6] discovered the kinematic bifurcation of the plane-symmetric Bricard linkage and the plane-symmetric spherical 6R linkage assembly. Ma et al. [7] obtained the bifurcation motion of the Bennett planar-spherical hybrid 6R mechanism. Song et al. [8] presented the constraint conditions of joints in a 6R metamorphic mechanism, which leads to eight motion branches and multiple furcation points. However, it is not easy to get analytical solutions of all the closed-loop equations of reconfigurable mechanisms. Some scholars use numerical methods to solve this problem where analytical solutions cannot be attained. Kumar and Pellegrino [9] developed a unique iterative algorithm to detect the existence of bifurcation motion based on the current configuration. Gan and Pellegrino [10] introduced the numerical solution of the closed-loop equation in the bifurcation detection of deployable structures.

Other scholars applied screw theory especially the screw system methods [11,12] to analyse the local motion characteristics of branch motions and constraints of different bifurcated motions. Gan et al. [13,14] used screw theory to study the mobility changes and bifurcated motion of novel metamorphic parallel mechanisms. Qin et al. [4] studied the multi-furcation phenomenon of the queer square mechanism, which can generate 14 bifurcation motion states through the constrained singular configuration. Gao et al. [15] presented a novel truss-shaped deployable grasping manipulator with mobility bifurcation, which changes its mobility from deployment to grasping motions.

Besides, there are other methods for revealing bifurcation in reconfigurable mechanisms. Wei and Dai [16,17] used the concept of Lie group to present the finite motion characteristics and differential manifold to explore the bifurcation phenomenon of reconfigurable parallel mechanisms. Wang and Wang [18] proposed an algorithm to determine all configuration branches and bifurcation points of the Stewart platform. Lee and Hervé [19] studied a 6R mechanism with two different single-degree-of-freedom motion modes and presented that bifurcation belongs to a special singularity type. Li and Hervé [20] designed a parallel mechanism with Schöenflie motion branches. Gogu [21] discussed the essence of bifurcation at the constraint singularity by using linear algebra method and expounded the relationship between constraint singularity and structural parameters of parallel mechanisms. Yuan et al. [22] introduced the concepts of mechanism stiffness and flexibility to define bifurcation motions. Nurahmi et al. [23] established the decomposition of constraint equations of 4-RUU parallel mechanism by using the algebraic method of Study's kinematic mapping of the Euclidean geometry group $SE(3)$ to analyse the reconfiguration.

High-order kinematics has been introduced to analyse the characteristics of mechanisms. Hunt [24] first applied the velocity screw to the construction of the first-order kinematic model of 6-DOF parallel mechanism, namely the velocity Jacobian matrix. This contribution has laid a solid theoretical foundation for much later research work. Generally, the first-order kinematic model can be directly obtained by deriving the position closed-loop equation [25–28]. Similarly, the second-order and higher-order kinematic models can also be obtained by directly deriving the first-order kinematic model [29–31]. Moreover, the method based on finite and instantaneous screw can be used to formulate the high-order kinematic models by directly differentiating the corresponding topology and velocity models, which is simple and straightforward with lower computation cost [32–35].

To simplify the mathematical model of higher-order kinematics, Joshi and Tsai proposed a general modelling method for non-overconstrained parallel mechanisms by using the property of reciprocal product of screws [36]. Thomas and Tesar proposed a general method to construct the acceleration model of the series kinematic chain by using the influence coefficient method [37]. Wang and Huang extended this method to the field of parallel mechanisms [38]. Staicu and Zhang revealed a recursive matrix method to represent the velocity and acceleration of the next configuration based on the velocity and acceleration model of the current configuration [39,40]. In 1996, Rico and Duffy proposed a simplified method to calculate the acceleration of spatial kinematic chains using screw theory [41]. Later, Rico et al. [42], Alvarado [43] extended this simplified method to the jerk and jounce analysis of spatial kinematic chains. Gallardo-Alvarado and Garcia-Murillo [44] applied the theory of screws in the jerk and hyper-jerk analyses of a six-degrees-of-freedom parallel manipulator. López-Custodio et al. [45] proposed a compact expression for high-order kinematic analysis and verified the equivalence with the expression derived by Lerbet in 1998 [46].

For the reconfigurable mechanisms, the current high-order kinematic analysis methods focus on the relationship between joint velocities at the singular configuration of mechanisms and have been used successfully on the revelation of bifurcation [47]. Here, we are going to reveal the bifurcation by establishing the high-order kinematic model and obtain the instantaneous joint velocities at the singular configuration of the mechanism, which can be obtained directly by the screw theory. Furthermore, with the screw theory, we can obtain the constraints of mechanisms if necessary. Hence, we adopt screw theory here instead of Lie group. In this paper, two special cases namely the Schatz-inspired metamorphic mechanisms are presented, where the first- and second-order based methods fail. Then, we propose a novel third- and fourth-order based method to reveal the bifurcation of the presented mechanism based on the simplified mathematical model of higher-order kinematics. The layout of this paper is as follows. Based on the geometric setup of Schatz-inspired metamorphic mechanism described in Sec. 2, two singular configurations are analysed with the first- and second-order based method in Sec. 3 and one of them cannot be revealed. Sec. 4 introduces the third- and fourth-order kinematics to obtain the acceleration constraint equations and illustrates the third- and fourth-order based method for the revelation of bifurcation, which leads to the motion branches given in Sec. 5. Then, this method is extended to another Schatz-inspired metamorphic mechanism in Sec. 6.

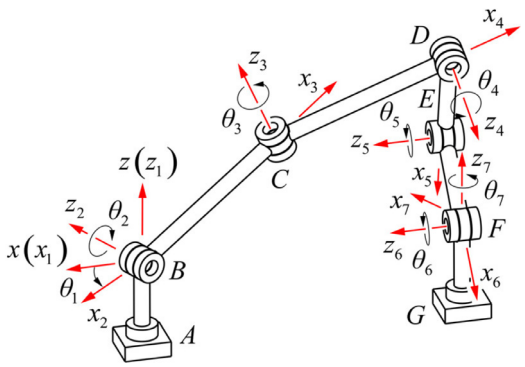

Fig. 1. The Schatz-inspired metamorphic mechanism.

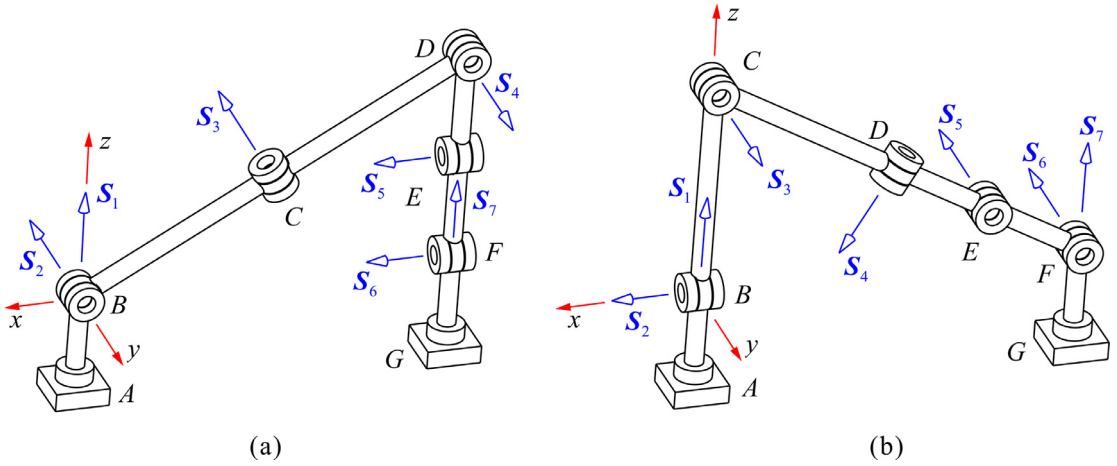

Fig. 2. Singular configuration I (a) and singular configuration II (b) of the Schatz-inspired metamorphic mechanism.

2. Geometric setup of the Schatz-inspired metamorphic mechanism

The Schatz-inspired metamorphic mechanism consists of seven links connected by seven revolute joints and one loop is constructed by these joints. As illustrated in Fig. 1, seven revolute joints are described by letters *A, B, C, D, E, F* and *G*, respectively. The Schatz-inspired metamorphic mechanism is a spatial 7R mechanism and can be seen as a Schatz linkage with an additional revolute joint *E*. The geometric parameters of the mechanism are

$$\begin{aligned} &a_{12} = a_{67} = 0, a_{23} = a_{34} = 2a, a_{45} = a_{56} = a, a_{71} = 2\sqrt{3}a \\ &\alpha_{12} = \alpha_{23} = \alpha_{34} = \alpha_{45} = \alpha_{67} = \pi/2, \alpha_{56} = \alpha_{71} = 0 \\ &R_2 = R_3 = R_4 = R_5 = R_6 = 0, R_1 = -R_7 = R \end{aligned} \tag{1}$$

The geometric setup of coordinate systems follows the Denavit and Hartenberg's convention [48]. The local coordinate system O_i-$x_iy_iz_i$ is established. Axis z_i lies along the revolute axis of joint i, axis x_i is collinear with the common normal direction pointing from axis z_{i-1} to axis z_i, axis y_i follows the right-handed rule. $a_{(i-1)i}$ is the link length representing the normal distance between axis z_{i-1} and axis z_i, $\alpha_{(i-1)i}$ is the twist angle from axis z_{i-1} to axis z_i about axis x_i, R_i is the joint offset representing the normal distance between axis x_i and axis x_{i+1}, and θ_i is the rotation angle from axis x_i to axis x_{i+1} about axis z_i. Here, link length $a_{(i-1)i}$, twist angle $\alpha_{(i-1)i}$, joint offset R_i and rotation angle θ_i are DH parameters in the mechanism.

The global coordinate system *B-xyz* is established with its origin at the centre point of joint *B* in Fig. 1. Axis *x* is collinear with axis x_1, axis *z* is collinear with axis z_1, axis *y* follows the right-handed rule.

When the Schatz-inspired metamorphic mechanism moves to a configuration that all links lie in the same plane, the mechanism is singular, and the configuration is called as singular configuration. As shown in Fig. 2, there are two singular configurations denoted as singular configuration I and singular configuration II, respectively.

Each of the seven revolute joints of the Schatz-inspired metamorphic mechanism as indicated in Fig. 2 is expressed by a screw, denoted as $\boldsymbol{S}_i$, which can represent the instantaneous velocity including linear velocity and angular velocity of a motion generated by a kinematic joint in the global coordinate system. Following Refs. [41–47], the dimension of the tangent cone equals to the local mobility of the mechanism at the singular configuration and the tangent cone can be approximated

by different order cones. For the revelation of bifurcation, we focus on the singular configuration, so we only establish the high-order kinematic model at the singular configuration rather than any one non-singular configuration in this paper. For the Schatz-inspired metamorphic mechanism, a can be 1 and R can be 0 for simplified calculation, because the axes of joints A and G are parallel to each other as shown in Fig. 1. Seven screws that are attached to the seven revolute joints at the singular configuration I in Fig. 2(a) can be calculated and written as

$$\begin{aligned}
&\boldsymbol{S}_1 = (0,0,1,0,0,0)^{\mathrm{T}}, \boldsymbol{S}_2 = (0,-1,0,0,0,0)^{\mathrm{T}}\\
&\boldsymbol{S}_3 = \left(\tfrac{1}{2},0,\tfrac{\sqrt{3}}{2},0,2,0\right)^{\mathrm{T}}, \boldsymbol{S}_4 = \left(0,1,0,-2,0,-2\sqrt{3}\right)^{\mathrm{T}}\\
&\boldsymbol{S}_5 = (1,0,0,0,1,0)^{\mathrm{T}}, \boldsymbol{S}_6 = (1,0,0,0,0,0)^{\mathrm{T}}\\
&\boldsymbol{S}_7 = \left(0,0,1,0,2\sqrt{3},0\right)^{\mathrm{T}}
\end{aligned} \tag{2}$$

Similarly, the seven screws at the singular configuration II in Fig. 2(b) can also be calculated and written as

$$\begin{aligned}
&\boldsymbol{S}_1 = (0,0,1,0,0,0)^{\mathrm{T}}, \boldsymbol{S}_2 = (1,0,0,0,0,0)^{\mathrm{T}}\\
&\boldsymbol{S}_3 = (0,1,0,-2,0,0)^{\mathrm{T}}, \boldsymbol{S}_4 = \left(\tfrac{1}{2},0,-\tfrac{\sqrt{3}}{2},0,-1,0\right)^{\mathrm{T}}\\
&\boldsymbol{S}_5 = \left(0,-1,0,\tfrac{1}{2},0,\tfrac{3\sqrt{3}}{2}\right)^{\mathrm{T}}, \boldsymbol{S}_6 = \left(0,-1,0,0,0,2\sqrt{3}\right)^{\mathrm{T}}\\
&\boldsymbol{S}_7 = \left(0,0,1,0,2\sqrt{3},0\right)^{\mathrm{T}}
\end{aligned} \tag{3}$$

3. First- and second-order kinematics

For the Schatz-inspired metamorphic mechanism, the closed-loop velocity equation can be expressed as

$$\omega_1\boldsymbol{S}_1 + \omega_2\boldsymbol{S}_2 + \omega_3\boldsymbol{S}_3 + \omega_4\boldsymbol{S}_4 + \omega_5\boldsymbol{S}_5 + \omega_6\boldsymbol{S}_6 + \omega_7\boldsymbol{S}_7 = \boldsymbol{0} \tag{4}$$

where ω_1, ω_2, ω_3, ω_4, ω_5, ω_6 and ω_7 represent the scalar angular velocities of revolute joints in the mechanism. Eq. (4) can be written in matrix form as

$$\boldsymbol{J\omega} = \begin{bmatrix} \boldsymbol{S}_1 & \boldsymbol{S}_2 & \boldsymbol{S}_3 & \boldsymbol{S}_4 & \boldsymbol{S}_5 & \boldsymbol{S}_6 & \boldsymbol{S}_7 \end{bmatrix} \begin{bmatrix} \omega_1\\ \omega_2\\ \omega_3\\ \omega_4\\ \omega_5\\ \omega_6\\ \omega_7 \end{bmatrix} = \boldsymbol{0} \tag{5}$$

Eq. (5) gives the Jacobian matrix of the mechanism which implements instantaneous velocity analysis for the mechanism when the mechanism moves from the singular configuration.

Substituting the seven screws of Eq. (2) into Eq. (5), the Jacobian matrix of singular configuration I in Fig. 2(a) can be expressed as a function of the mechanism dimensions and the first-order velocity constraint equations of the mechanism at singular configuration I are obtained as

$$\boldsymbol{J\omega} = \begin{bmatrix} 0 & 0 & \frac{1}{2} & 0 & 1 & 1 & 0\\ 0 & -1 & 0 & 1 & 0 & 0 & 0\\ 1 & 0 & \frac{\sqrt{3}}{2} & 0 & 0 & 0 & 1\\ 0 & 0 & 0 & -2 & 0 & 0 & 0\\ 0 & 0 & 2 & 0 & 1 & 0 & 2\sqrt{3}\\ 0 & 0 & 0 & -2\sqrt{3} & 0 & 0 & 0 \end{bmatrix} \begin{bmatrix} \omega_1\\ \omega_2\\ \omega_3\\ \omega_4\\ \omega_5\\ \omega_6\\ \omega_7 \end{bmatrix} = \boldsymbol{0} \tag{6}$$

The dimension of matrix $\boldsymbol{J}$ is 6×7 since the mechanism has only one loop and seven joints. It can be found that the fourth and sixth rows of the Jacobian matrix in Eq. (6) are dependent. Then, the first-order velocity constraint equations can be simplified as

$$\boldsymbol{J\omega} = \begin{bmatrix} 0 & 0 & \frac{1}{2} & 0 & 1 & 1 & 0\\ 0 & -1 & 0 & 1 & 0 & 0 & 0\\ 1 & 0 & \frac{\sqrt{3}}{2} & 0 & 0 & 0 & 1\\ 0 & 0 & 0 & -2 & 0 & 0 & 0\\ 0 & 0 & 2 & 0 & 1 & 0 & 2\sqrt{3} \end{bmatrix} \begin{bmatrix} \omega_1\\ \omega_2\\ \omega_3\\ \omega_4\\ \omega_5\\ \omega_6\\ \omega_7 \end{bmatrix} = \boldsymbol{0} \tag{7}$$

It shows that the rank of matrix $\boldsymbol{J}$ is 5. There are 7 angular velocity variables and the transitory mobility of the mechanism at singular configuration I is 2.

When we take derivatives of both sides of Eq. (4) to implement acceleration analysis for the Schatz-inspired metamorphic mechanism, the closed-loop acceleration equation [42,49] is obtained as

$$\alpha_1\boldsymbol{S}_1+\alpha_2\boldsymbol{S}_2+\alpha_3\boldsymbol{S}_3+\alpha_4\boldsymbol{S}_4+\alpha_5\boldsymbol{S}_5+\alpha_6\boldsymbol{S}_6+\alpha_7\boldsymbol{S}_7=-\boldsymbol{S}_L \tag{8}$$

where α_1, α_2, α_3, α_4, α_5, α_6 and α_7 represent the scalar angular accelerations of revolute joints in the mechanism. The Lie screw $\boldsymbol{S}_L$ [47] can be computed by a sequential operation using the Lie bracket of screws and expressed in bilinear form as

$$\begin{aligned}\boldsymbol{S}_L&=\sum_{i<j}\omega_i\omega_j\left[\boldsymbol{S}_i,\boldsymbol{S}_j\right]\\&=\begin{bmatrix}\omega_1\\\omega_2\\\omega_3\\\omega_4\\\omega_5\\\omega_6\\\omega_7\end{bmatrix}^{\mathrm{T}}\begin{bmatrix}\mathbf{0}&[\boldsymbol{S}_1,\boldsymbol{S}_2]&[\boldsymbol{S}_1,\boldsymbol{S}_3]&[\boldsymbol{S}_1,\boldsymbol{S}_4]&[\boldsymbol{S}_1,\boldsymbol{S}_5]&[\boldsymbol{S}_1,\boldsymbol{S}_6]&[\boldsymbol{S}_1,\boldsymbol{S}_7]\\\mathbf{0}&\mathbf{0}&[\boldsymbol{S}_2,\boldsymbol{S}_3]&[\boldsymbol{S}_2,\boldsymbol{S}_4]&[\boldsymbol{S}_2,\boldsymbol{S}_5]&[\boldsymbol{S}_2,\boldsymbol{S}_6]&[\boldsymbol{S}_2,\boldsymbol{S}_7]\\\mathbf{0}&\mathbf{0}&\mathbf{0}&[\boldsymbol{S}_3,\boldsymbol{S}_4]&[\boldsymbol{S}_3,\boldsymbol{S}_5]&[\boldsymbol{S}_3,\boldsymbol{S}_6]&[\boldsymbol{S}_3,\boldsymbol{S}_7]\\\mathbf{0}&\mathbf{0}&\mathbf{0}&\mathbf{0}&[\boldsymbol{S}_4,\boldsymbol{S}_5]&[\boldsymbol{S}_4,\boldsymbol{S}_6]&[\boldsymbol{S}_4,\boldsymbol{S}_7]\\\mathbf{0}&\mathbf{0}&\mathbf{0}&\mathbf{0}&\mathbf{0}&[\boldsymbol{S}_5,\boldsymbol{S}_6]&[\boldsymbol{S}_5,\boldsymbol{S}_7]\\\mathbf{0}&\mathbf{0}&\mathbf{0}&\mathbf{0}&\mathbf{0}&\mathbf{0}&[\boldsymbol{S}_6,\boldsymbol{S}_7]\\\mathbf{0}&\mathbf{0}&\mathbf{0}&\mathbf{0}&\mathbf{0}&\mathbf{0}&\mathbf{0}\end{bmatrix}\begin{bmatrix}\omega_1\\\omega_2\\\omega_3\\\omega_4\\\omega_5\\\omega_6\\\omega_7\end{bmatrix}\end{aligned} \tag{9}$$

where $1\le i<j\le 7$. The rule of calculating the Lie bracket of any two screws $\boldsymbol{S}_i$ and $\boldsymbol{S}_j$ can be given as

$$\left[\boldsymbol{S}_i,\boldsymbol{S}_j\right]=\begin{pmatrix}\boldsymbol{s}_i\times\boldsymbol{s}_j\\\boldsymbol{s}_i\times\boldsymbol{s}_{j0}+\boldsymbol{s}_{i0}\times\boldsymbol{s}_j\end{pmatrix} \tag{10}$$

where the 3-dimensional vectors $\boldsymbol{s}_i$ and $\boldsymbol{s}_j$ are the primary parts of screws $\boldsymbol{S}_i$ and $\boldsymbol{S}_j$ respectively, while the 3-dimensional vectors $\boldsymbol{s}_{i0}$ and $\boldsymbol{s}_{j0}$ are the secondary parts of screws $\boldsymbol{S}_i$ and $\boldsymbol{S}_j$ respectively. The Lie bracket formula satisfies anti-commutativity which is $[\boldsymbol{S}_i, \boldsymbol{S}_j] = -[\boldsymbol{S}_j, \boldsymbol{S}_i]$.

For singular configuration I, substituting the seven screws of Eq. (2) into Eq. (9), the Lie screw $\boldsymbol{S}_L$ can be expressed as

$$\boldsymbol{S}_L=\begin{pmatrix}\omega_1(\omega_2-\omega_4)-\omega_2\left(\frac{\sqrt{3}}{2}\omega_3+\omega_7\right)-\frac{\sqrt{3}}{2}\omega_3\omega_4+\omega_4\omega_7\\\omega_1\left(\frac{1}{2}\omega_3+\omega_5+\omega_6\right)+\omega_3\left(\frac{\sqrt{3}}{2}\omega_5+\frac{\sqrt{3}}{2}\omega_6-\frac{1}{2}\omega_7\right)-\omega_7(\omega_5+\omega_6)\\\omega_2\left(\frac{1}{2}\omega_3+\omega_5+\omega_6\right)+\frac{1}{2}\omega_3\omega_4-\omega_4(\omega_5+\omega_6)\\-\omega_1\left(2\omega_3+\omega_5+2\sqrt{3}\omega_7\right)+2\sqrt{3}\omega_2\omega_4-\omega_3\left(\frac{\sqrt{3}}{2}\omega_5+\omega_7\right)+\omega_5\omega_7\\-2\omega_1\omega_4-2\omega_4\left(\sqrt{3}\omega_5+\sqrt{3}\omega_6-\omega_7\right)\\-2\omega_2\omega_4+\omega_3\left(-\frac{3}{2}\omega_5-2\omega_6+\sqrt{3}\omega_7\right)-\omega_5\omega_6+2\sqrt{3}\omega_7(\omega_5+\omega_6)\end{pmatrix} \tag{11}$$

Then, substituting the first-order velocity constraint equations in Eq. (7), Eq. (11) can be simplified as

$$\boldsymbol{S}_L=\begin{pmatrix}0\\-\frac{\sqrt{3}}{4}\omega_3^2\\0\\\sqrt{3}\omega_3^2-2\sqrt{3}\omega_7^2\\0\\\omega_3^2+\omega_5^2+\omega_3\omega_5\end{pmatrix} \tag{12}$$

Eq. (8) can also be written in matrix form as

$$\boldsymbol{J}\boldsymbol{\alpha}=\begin{bmatrix}\boldsymbol{S}_1&\boldsymbol{S}_2&\boldsymbol{S}_3&\boldsymbol{S}_4&\boldsymbol{S}_5&\boldsymbol{S}_6&\boldsymbol{S}_7\end{bmatrix}\begin{bmatrix}\alpha_1\\\alpha_2\\\alpha_3\\\alpha_4\\\alpha_5\\\alpha_6\\\alpha_7\end{bmatrix}=-\boldsymbol{S}_L \tag{13}$$

The algebraic condition for solving Eq. (13) can be expressed as

$$\mathrm{Rank}(\boldsymbol{J})=\mathrm{Rank}\left(\begin{bmatrix}\boldsymbol{J}&-\boldsymbol{S}_L\end{bmatrix}\right) \tag{14}$$

Eq. (7) shows that Rank ($\boldsymbol{J}$) = 5. Then, Rank ([$\boldsymbol{J}$ $-\boldsymbol{S}_L$]) = 5, which means that all the six-order cofactors of the extended matrix [$\boldsymbol{J}$ $-\boldsymbol{S}_L$] are zero [50]. Thus, the second-order velocity constraint equations of the Schatz-inspired metamorphic mechanism can be obtained by calculating all the six-order cofactors of the augmented matrix as

$$-2\omega_3^2+\omega_3\omega_5+\omega_5^2+6\omega_7^2=0 \tag{15}$$

Assembling the first-order velocity constraint equations in Eq. (7) and the second-order velocity constraint equations in Eq. (15), the following constraint system with first- and second-order velocity constraints integrated is obtained and all possible constraints exerted to the mechanism at singular configuration I can be listed as

$$\begin{cases} \frac{1}{2}\omega_3+\omega_5+\omega_6=0 \\ -\omega_2+\omega_4=0 \\ \omega_1+\frac{\sqrt{3}}{2}\omega_3+\omega_7=0 \\ -2\omega_4=0 \\ 2\omega_3+\omega_5+2\sqrt{3}\omega_7=0 \\ -2\omega_3^2+\omega_3\omega_5+\omega_5^2+6\omega_7^2=0 \end{cases} \tag{16}$$

Considering the constraint system of the Schatz-inspired metamorphic mechanism presented in Eq. (16), two linearly independent solutions are obtained. For the mechanisms in this paper, two linearly independent solutions, namely, two high-order cones at the singular configuration are corresponded to two finite motion braches. If representing these solutions in the form of 7-dimensional column vectors $(\omega_1\ \omega_2\ \ldots\ \omega_7)^{\mathrm{T}}$, the solution vectors can be expressed as

$$\left(\frac{\sqrt{3}}{3}\omega_6 \quad 0 \quad -2\omega_6 \quad 0 \quad 0 \quad \omega_6 \quad \frac{2\sqrt{3}}{3}\omega_6 \right)^{\mathrm{T}} \tag{17}$$

$$\left(-\frac{\sqrt{3}}{3}\omega_6 \quad 0 \quad \frac{2}{3}\omega_6 \quad 0 \quad -\frac{4}{3}\omega_6 \quad \omega_6 \quad 0 \right)^{\mathrm{T}} \tag{18}$$

Similar to singular configuration I in Fig. 2(a), substituting the seven screws of Eq. (3) into Eq. (5), first-order velocity constraint equations of the Schatz-inspired metamorphic mechanism at singular configuration II in Fig. 2(b) are obtained as

$$\boldsymbol{J\omega}=\begin{bmatrix} 0 & 1 & 0 & \frac{1}{2} & 0 & 0 & 0 \\ 0 & 0 & 1 & 0 & -1 & -1 & 0 \\ 1 & 0 & 0 & -\frac{\sqrt{3}}{2} & 0 & 0 & 1 \\ 0 & 0 & -2 & 0 & \frac{1}{2} & 0 & 0 \\ 0 & 0 & 0 & -1 & 0 & 0 & 2\sqrt{3} \\ 0 & 0 & 0 & 0 & \frac{3\sqrt{3}}{2} & 2\sqrt{3} & 0 \end{bmatrix}\begin{bmatrix} \omega_1 \\ \omega_2 \\ \omega_3 \\ \omega_4 \\ \omega_5 \\ \omega_6 \\ \omega_7 \end{bmatrix}=\mathbf{0} \tag{19}$$

Substituting the seven screws of Eq. (3) into Eq. (9), the Lie screw $\boldsymbol{S}_L$ of singular configuration II can be expressed and simplified as

$$\boldsymbol{S}_L=\begin{pmatrix} -\sqrt{3}\omega_3\omega_4 \\ \frac{\sqrt{3}}{2}\omega_2\omega_4 \\ -\omega_3\omega_4 \\ 2\omega_4\omega_7-\frac{\sqrt{3}}{2}\omega_5\omega_6 \\ -2\sqrt{3}\omega_3\omega_4 \\ \sqrt{3}\omega_4\omega_7-\frac{1}{2}\omega_5\omega_6 \end{pmatrix} \tag{20}$$

The augmented matrix of Eq. (13) at singular configuration II is

$$\begin{bmatrix} 0 & 1 & 0 & \frac{1}{2} & 0 & 0 & 0 & \sqrt{3}\omega_3\omega_4 \\ 0 & 0 & 1 & 0 & -1 & -1 & 0 & -\frac{\sqrt{3}}{2}\omega_2\omega_4 \\ 1 & 0 & 0 & -\frac{\sqrt{3}}{2} & 0 & 0 & 1 & \omega_3\omega_4 \\ 0 & 0 & -2 & 0 & \frac{1}{2} & 0 & 0 & -2\omega_4\omega_7+\frac{\sqrt{3}}{2}\omega_5\omega_6 \\ 0 & 0 & 0 & -1 & 0 & 0 & 2\sqrt{3} & 2\sqrt{3}\omega_3\omega_4 \\ 0 & 0 & 0 & 0 & \frac{3\sqrt{3}}{2} & 2\sqrt{3} & 0 & -\sqrt{3}\omega_4\omega_7+\frac{1}{2}\omega_5\omega_6 \end{bmatrix} \tag{21}$$

Thus, the second-order velocity constraint equations of the Schatz-inspired metamorphic mechanism at singular configuration II in Fig. 2(b) can be obtained by calculating all the six-order cofactors of the augmented matrix as

$$3\omega_2\omega_4-2\omega_5\omega_6+3\sqrt{3}\omega_4\omega_7=0 \tag{22}$$

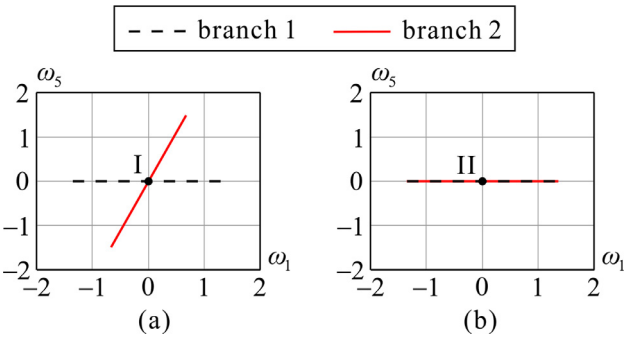

Fig. 3. The relation of angular velocities$\omega_5$vs$\omega_1$at singular configuration I (a) and singular configuration II (b).

Then, the following constraint system with first and second-order kinematics is obtained as

$$\begin{cases} \omega_2 + \frac{1}{2}\omega_4 = 0 \\ \omega_3 - \omega_5 - \omega_6 = 0 \\ \omega_1 - \frac{\sqrt{3}}{2}\omega_4 + \omega_7 = 0 \\ -2\omega_3 + \frac{1}{2}\omega_5 = 0 \\ -\omega_4 + 2\sqrt{3}\omega_7 = 0 \\ 3\omega_2\omega_4 - 2\omega_5\omega_6 + 3\sqrt{3}\omega_4\omega_7 = 0 \end{cases} \tag{23}$$

Considering the constraint system of the mechanism presented in Eq. (23), only one linearly independent solution is obtained. If representing it in a 7-dimensional column vector $(\omega_1\ \omega_2\ \omega_3\ \omega_4\ \omega_5\ \omega_6\ \omega_7)^{\mathrm{T}}$, the solution vector can be expressed as

$$\begin{pmatrix} 2\omega_7 & -\sqrt{3}\omega_7 & 0 & 2\sqrt{3}\omega_7 & 0 & 0 & \omega_7 \end{pmatrix}^{\mathrm{T}} \tag{24}$$

Comparing Eqs. (17)(18) and Eq. (24), it can be found that there are two linearly independent solutions, which means there are two different motion branches that can be revealed through the first- and second-order based method at singular configuration I in Fig. 2(a). However, there is only one linearly independent solution and it cannot be revealed whether there are different motion branches at singular configuration II in Fig. 2(b), of which the reason is that the two motion branches have the same velocity at singular configuration II as shown in Fig. 3(b). Fig. 3 presents the angular velocity relationship of two different motion branches at the singular configurations, which are obtained by the first- and second-order constraint equations. Moreover, the angular velocity relationship is also the tangent of the motion curves at the singular configurations. In other words, the kinematic curves of these two motion branches are tangent at singular configuration II in Fig. 3(b). Meanwhile, as shown in Fig. 3(a), the two motion branches have different velocities and the kinematic curves of these two motion branches intersect at singular configuration I.

In a word, the first- and second-order based method succeeds in the revelation of different motion branches at singular configuration I but fails to reveal different motion branches at singular configuration II. Here, it cannot be determined whether there is no bifurcation or two tangential motion branches. The difference is that the former has only one curvature but the latter has two different curvatures, namely different acceleration relations. Then, it needs to calculate the acceleration relation of kinematic joints at singular configuration II in the following section.

4. Third- and fourth-order kinematics

In Sec. 3, we have obtained the second-order acceleration constraint equations at singular configuration II as Eq. (13). Substituting Eqs. (3), (20) and (24), it can be written as

$$\boldsymbol{J\alpha} = \begin{bmatrix} 0 & 1 & 0 & \frac{1}{2} & 0 & 0 & 0 \\ 0 & 0 & 1 & 0 & -1 & -1 & 0 \\ 1 & 0 & 0 & -\frac{\sqrt{3}}{2} & 0 & 0 & 1 \\ 0 & 0 & -2 & 0 & \frac{1}{2} & 0 & 0 \\ 0 & 0 & 0 & -1 & 0 & 0 & 2\sqrt{3} \\ 0 & 0 & 0 & 0 & \frac{3\sqrt{3}}{2} & 2\sqrt{3} & 0 \end{bmatrix} \begin{bmatrix} \alpha_1 \\ \alpha_2 \\ \alpha_3 \\ \alpha_4 \\ \alpha_5 \\ \alpha_6 \\ \alpha_7 \end{bmatrix} = \begin{pmatrix} 0 \\ 3\sqrt{3}\omega_7^2 \\ 0 \\ -4\sqrt{3}\omega_7^2 \\ 0 \\ -6\omega_7^2 \end{pmatrix} \tag{25}$$

Then, we need to calculate the third-order kinematics to obtain other acceleration constraint equations. When we take derivatives of both sides of Eq. (8) to implement jerk analysis for the Schatz-inspired metamorphic mechanism, the closed-loop jerk equation is obtained as

$$\rho_1\boldsymbol{S}_1+\rho_2\boldsymbol{S}_2+\rho_3\boldsymbol{S}_3+\rho_4\boldsymbol{S}_4+\rho_5\boldsymbol{S}_5+\rho_6\boldsymbol{S}_6+\rho_7\boldsymbol{S}_7=-\boldsymbol{S}_J \tag{26}$$

where ρ_1, ρ_2, ρ_3, ρ_4, ρ_5, ρ_6 and ρ_7 represent the scalar angular jerks of revolute joints in the mechanism. The jerk screw $\boldsymbol{S}_J$ [45] can be computed by a sequential operation using the Lie bracket of screws and expressed as

$$\begin{aligned}\boldsymbol{S}_J=&2\sum_{i<j}\omega_i\alpha_j\left[\boldsymbol{S}_i,\boldsymbol{S}_j\right]+\sum_{i<j}\alpha_i\omega_j\left[\boldsymbol{S}_i,\boldsymbol{S}_j\right]\\&+\sum_{i<j}\omega_i\omega_i\omega_j\left[\boldsymbol{S}_i,\left[\boldsymbol{S}_i,\boldsymbol{S}_j\right]\right]+2\sum_{i<j<k}\omega_i\omega_j\omega_k\left[\boldsymbol{S}_i,\left[\boldsymbol{S}_j,\boldsymbol{S}_k\right]\right]\end{aligned} \tag{27}$$

where the detailed items are placed in the Appendix. Then, the jerk screw $\boldsymbol{S}_J$ can be written as

$$\boldsymbol{S}_J=\begin{bmatrix}-(6\alpha_3+3\alpha_5+3\alpha_6)\omega_7+9\sqrt{3}\omega_7^3\\(6\alpha_2-\frac{3}{2}\alpha_4)\omega_7\\-3\sqrt{3}\alpha_3\omega_7+9\omega_7^3\\6\alpha_4\omega_7\\-(12\alpha_3+\frac{3}{2}\alpha_5)\omega_7+10\sqrt{3}\omega_7^3\\3\sqrt{3}\alpha_4\omega_7\end{bmatrix} \tag{28}$$

Eq. (26) can also be written in matrix form as

$$\boldsymbol{J}\boldsymbol{\rho}=\begin{bmatrix}\boldsymbol{S}_1&\boldsymbol{S}_2&\boldsymbol{S}_3&\boldsymbol{S}_4&\boldsymbol{S}_5&\boldsymbol{S}_6&\boldsymbol{S}_7\end{bmatrix}\begin{bmatrix}\rho_1\\\rho_2\\\rho_3\\\rho_4\\\rho_5\\\rho_6\\\rho_7\end{bmatrix}=-\boldsymbol{S}_J \tag{29}$$

The algebraic condition for solving Eq. (29) can be expressed as

$$\mathrm{Rank}(\boldsymbol{J})=\mathrm{Rank}\left(\begin{bmatrix}\boldsymbol{J}&-\boldsymbol{S}_J\end{bmatrix}\right) \tag{30}$$

Similar to Eq. (14), Rank ([$\boldsymbol{J}$ –$\boldsymbol{S}_J$]) = 5, which also means that all the six-order cofactors of the extended matrix [$\boldsymbol{J}$ – $\boldsymbol{S}_J$] are zero. Thus, the third-order acceleration constraint equations of the Schatz-inspired metamorphic mechanism can be obtained by calculating all the six-order cofactors of the extended matrix as

$$\omega_7(2\alpha_2+\alpha_4)=0 \tag{31}$$

Comparing Eq. (31) and the first second-order acceleration constraint equation in Eq. (25), we can find that these two equations are equivalent to each other, which means that the third-order acceleration constraint equation cannot be used for the revelation of bifurcation. Further, we need to calculate the fourth-order kinematics to attain other acceleration constraint equations as follows.

Taking derivatives of both sides of Eq. (26) to implement jounce analysis for the Schatz-inspired metamorphic mechanism, the closed-loop jounce equation is obtained as

$$\tau_1\boldsymbol{S}_1+\tau_2\boldsymbol{S}_2+\tau_3\boldsymbol{S}_3+\tau_4\boldsymbol{S}_4+\tau_5\boldsymbol{S}_5+\tau_6\boldsymbol{S}_6+\tau_7\boldsymbol{S}_7=-\boldsymbol{S}_{J0} \tag{32}$$

where τ_1, τ_2, τ_3, τ_4, τ_5, $\tau_6$and τ_7 represent the scalar angular jounces of revolute joints in the mechanism. The jounce screw $\boldsymbol{S}_{J0}$ [45] can be computed by a sequential operation using the Lie bracket of screws and expressed as

$$\begin{aligned}\boldsymbol{S}_{J0}=&3\sum_{i<j}\omega_i\rho_j\left[\boldsymbol{S}_i,\boldsymbol{S}_j\right]+\sum_{i<j}\rho_i\omega_j\left[\boldsymbol{S}_i,\boldsymbol{S}_j\right]+3\sum_{i<j}\alpha_i\alpha_j\left[\boldsymbol{S}_i,\boldsymbol{S}_j\right]\\&+3\sum_{i<j}\omega_i\omega_i\alpha_j\left[\boldsymbol{S}_i,\left[\boldsymbol{S}_i,\boldsymbol{S}_j\right]\right]+3\sum_{i<j}\omega_i\alpha_i\omega_j\left[\boldsymbol{S}_i,\left[\boldsymbol{S}_i,\boldsymbol{S}_j\right]\right]+6\sum_{i<j<k}\omega_i\omega_j\alpha_k\left[\boldsymbol{S}_i,\left[\boldsymbol{S}_j,\boldsymbol{S}_k\right]\right]\\&+3\sum_{i<j<k}\omega_i\alpha_j\omega_k\left[\boldsymbol{S}_i,\left[\boldsymbol{S}_j,\boldsymbol{S}_k\right]\right]+3\sum_{i<j<k}\alpha_i\omega_j\omega_k\left[\boldsymbol{S}_i,\left[\boldsymbol{S}_j,\boldsymbol{S}_k\right]\right]\\&+\sum_{i<j}\omega_i\omega_i\omega_i\omega_j\left[\boldsymbol{S}_i,\left[\boldsymbol{S}_i,\left[\boldsymbol{S}_i,\boldsymbol{S}_j\right]\right]\right]+3\sum_{i<j<k}\omega_i\omega_i\omega_j\omega_k\left[\boldsymbol{S}_i,\left[\boldsymbol{S}_i,\left[\boldsymbol{S}_j,\boldsymbol{S}_k\right]\right]\right]\\&+3\sum_{i<j<k}\omega_i\omega_j\omega_j\omega_k\left[\boldsymbol{S}_i,\left[\boldsymbol{S}_j,\left[\boldsymbol{S}_j,\boldsymbol{S}_k\right]\right]\right]+6\sum_{h<i<j<k}\omega_h\omega_i\omega_j\omega_k\left[\boldsymbol{S}_h,\left[\boldsymbol{S}_i,\left[\boldsymbol{S}_j,\boldsymbol{S}_k\right]\right]\right]\end{aligned} \tag{33}$$

where the detailed items are placed in the Appendix. Then, the jounce screw $\boldsymbol{S}_{J0}$ can be written as

$$\boldsymbol{S}_{J0}=\begin{bmatrix} -(8\rho_3+4\rho_5+4\rho_6)\omega_7+6\sqrt{3}\alpha_2\alpha_3-72\alpha_2\omega_7^2 \\ (8\rho_2-2\rho_4)\omega_7-3\sqrt{3}\alpha_2^2-36\alpha_3\omega_7^2+18\sqrt{3}\omega_7^4 \\ -4\sqrt{3}\rho_3\omega_7+6\alpha_2\alpha_3-18\sqrt{3}\alpha_2\omega_7^2 \\ 8\rho_4\omega_7+4\sqrt{3}\alpha_2^2+18\sqrt{3}\alpha_3^2-144\alpha_3\omega_7^2+144\sqrt{3}\omega_7^4 \\ -(16\rho_3+2\rho_5)\omega_7+12\sqrt{3}\alpha_2\alpha_3-84\alpha_2\omega_7^2 \\ 4\sqrt{3}\rho_4\omega_7+6\alpha_2^2+18\alpha_3^2-72\sqrt{3}\alpha_3\omega_7^2+324\omega_7^4 \end{bmatrix} \tag{34}$$

Eq. (32) can also be written in matrix form as

$$\boldsymbol{J}\boldsymbol{\tau}=\begin{bmatrix} \boldsymbol{S}_1 & \boldsymbol{S}_2 & \boldsymbol{S}_3 & \boldsymbol{S}_4 & \boldsymbol{S}_5 & \boldsymbol{S}_6 & \boldsymbol{S}_7 \end{bmatrix}\begin{bmatrix} \tau_1 \\ \tau_2 \\ \tau_3 \\ \tau_4 \\ \tau_5 \\ \tau_6 \\ \tau_7 \end{bmatrix}=-\boldsymbol{S}_{J0} \tag{35}$$

The algebraic condition for solving Eq. (35) can be expressed as

$$\mathrm{Rank}(\boldsymbol{J})=\mathrm{Rank}\left(\begin{bmatrix} \boldsymbol{J} & -\boldsymbol{S}_{J0} \end{bmatrix}\right) \tag{36}$$

Similar to Eq. (14) and (30), Rank ($[\boldsymbol{J}\ -\boldsymbol{S}_{J0}]$) = 5, which means that all the six-order cofactors of the extended matrix $[\boldsymbol{J}\ -\boldsymbol{S}_{J0}]$ are zero. Thus, the fourth-order acceleration constraint equations of the Schatz-inspired metamorphic mechanism can be obtained by calculating all the six-order cofactors of the extended matrix as

$$2\rho_2\omega_7+\rho_4\omega_7+3\sqrt{3}\alpha_3^2+36\sqrt{3}\omega_7^4-36\alpha_3\omega_7^2=0 \tag{37}$$

From Eq. (29), we can get the relation equation of ρ_2 and ρ_4 as

$$\rho_2+\frac{1}{2}\rho_4=(6\alpha_3+3\alpha_5+3\alpha_6)\omega_7-9\sqrt{3}\omega_7^3 \tag{38}$$

Then, substituting Eq. (38) and (25) into Eq. (37), it can be simplified as

$$\alpha_3\left(\alpha_3-2\sqrt{3}\omega_7^2\right)=0 \tag{39}$$

From the above constraint system and rearranging the fourth-order acceleration constraints, all possible constraints exerted to the mechanism at the singular configuration can be listed as

$$\begin{cases} \alpha_2+\frac{1}{2}\alpha_4=0 \\ \alpha_3-\alpha_5-\alpha_6=3\sqrt{3}\omega_7^2 \\ \alpha_1-\frac{\sqrt{3}}{2}\alpha_4+\alpha_7=0 \\ -2\alpha_3+\frac{1}{2}\alpha_5=-4\sqrt{3}\omega_7^2 \\ -\alpha_4+2\sqrt{3}\alpha_7=0 \\ \frac{3\sqrt{3}}{2}\alpha_5+2\sqrt{3}\alpha_6=-6\omega_7^2 \\ \alpha_3\left(\alpha_3-2\sqrt{3}\omega_7^2\right)=0 \end{cases} \tag{40}$$

Considering the constraint system of the mechanism presented in Eq. (40), two linearly independent solutions are obtained. If representing these solutions in the form of 7-dimensional column vectors $(\alpha_1\ \alpha_2\ \ldots\ \alpha_7)^{\mathrm{T}}$, the solution vectors can be expressed as

$$\left(\ -\frac{2\sqrt{3}}{3}\alpha_2\ \ \alpha_2\ \ 2\sqrt{3}\omega_7^2\ \ -2\alpha_2\ \ 0\ \ -\sqrt{3}\omega_7^2\ \ -\frac{\sqrt{3}}{3}\alpha_2\ \right)^{\mathrm{T}} \tag{41}$$

$$\left(\ -\frac{2\sqrt{3}}{3}\alpha_2\ \ \alpha_2\ \ 0\ \ -2\alpha_2\ \ -8\sqrt{3}\omega_7^2\ \ 5\sqrt{3}\omega_7^2\ \ -\frac{\sqrt{3}}{3}\alpha_2\ \right)^{\mathrm{T}} \tag{42}$$

These two linearly independent solutions correspond to two different motion branches revealed by the third- and fourth-order based method. Fig. 4 presents the angular acceleration relationship of two different motion branches at the singular configurations, which are obtained by the third- and fourth-order constraint equations. Moreover, the angular acceleration relationship describes the curvature of the motion curves at the singular configuration. Considering these two relations of joint angular accelerations in Eqs. (41) and (42) as shown in Fig. 4 with the relation of angular velocities in Eq. (24) at singular configuration II, the difference between these two motion branches is that revolute joint E is geometrically constrained in one motion branch while not geometrically constrained in the other motion branch. In other words, when the

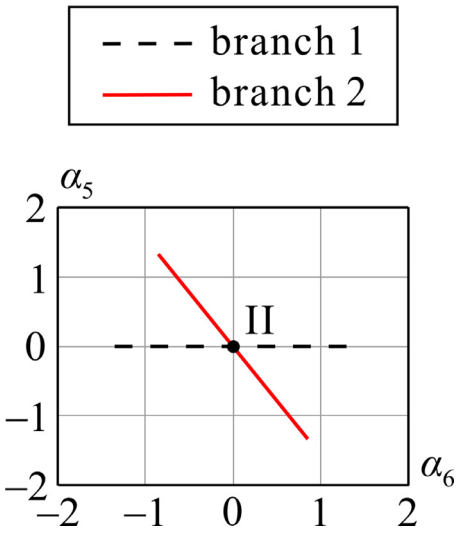

Fig. 4. The relation of angular accelerations$\alpha_5$vs$\alpha_6$at singular configuration II.

Schatz-inspired metamorphic mechanism moves through singular configuration II in Fig. 3(b), the curvatures of kinematic curves of these two motion branches are different, although the tangent lines of them are the same.

For this mechanism in the paper, its configuration space is seven-dimensional. Here, we choose the two-dimensional graphs to illustrate the relationship of angular velocities and angular accelerations. Any two of the seven joints can be selected in the two-dimensional graphs. We just choose two of them as an example to illustrate. Ideally, choosing the same joints is better for the consistency of the figures. However, in Fig. 4, the angular accelerations and angular velocities of joints *A* and *E* are coupled, making it unable to present the relationship of angular accelerations in a numerical way, so we choose joints *E* and *F* instead of joints *A* and *E*.

5. Motion branches in the Schatz-inspired metamorphic mechanism

In the previous sections, we have revealed all the motion branches and singular configurations in the Schatz-inspired metamorphic mechanism as shown in Fig. 5, where I-III-II-IV-I correspond to configurations of the mechanism along motion branch 1 and I-V-II-VI-I correspond to configurations of the mechanism along motion branch 2.

For the motion branches in Fig. 5, joint *E* is geometrically constrained in motion branch 1, where the mechanism moves as a Schatz mechanism, but not geometrically constrained in motion branch 2, where the mechanism moves as a single degree-of-freedom spatial 7R mechanism. Moreover, the kinematic curves of these motion branches intersect at singular configuration I and are tangent with different curvatures at singular configuration II. When the mechanism moves to singular configurations, the mechanism will be divided into two motion branches and this is coined as bifurcation. The mechanism can switch its motion branches when going through the intersection points and these points can thus be coined as constraint singularity. It can realise the reconfigurable switch between these two motion branches through singular configuration I and singular configuration II.

6. Extension to another Schatz-inspired metamorphic mechanism

Most of the existing metamorphic mechanisms can be analyzed with the first- and second-order based methods and their motion branches intersect at the bifurcation points. Besides the above-mentioned mechanism, another Schatz-inspired metamorphic mechanism is used to present the third- and fourth-order based method for its bifurcation revelation using screw theory. These two mechanisms are both spatial 7R mechanisms and can be seen as Schatz mechanisms with additional revolute joints. The positions and orientations of the axes of the additional revolute joints are different in these two mechanisms, which induce the different geometric parameters of the mechanisms. The geometric parameters of the mechanism are

$$\begin{aligned} &a_{12} = a_{67} = 0, a_{23} = a_{56} = 2a, a_{34} = a_{45} = a, a_{71} = 2\sqrt{3}a \\ &\alpha_{12} = \alpha_{23} = \alpha_{34} = \alpha_{56} = \alpha_{67} = \pi/2, \alpha_{45} = \alpha_{71} = 0 \\ &R_2 = R_3 = R_4 = R_5 = R_6 = 0, R_1 = -R_7 = R \end{aligned} \tag{43}$$

The global coordinate system *B*-*xyz* is established with its origin at the centre point of joint *B* in Fig. 6. Axis *x* is collinear with axis x_1, axis *z* is collinear with axis z_1, axis *y* follows the right-handed rule. Similarly, there are two singular configurations denoted as singularity configuration I and singular configuration II as shown in Fig. 7, respectively.

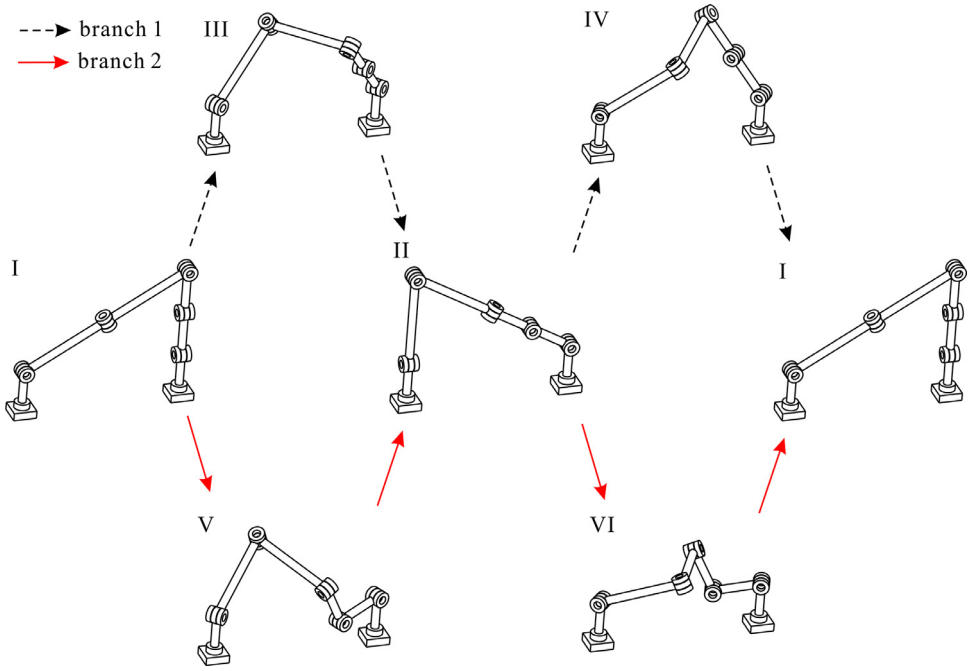

Fig. 5. Motion branches of the Schatz-inspired metamorphic mechanism.

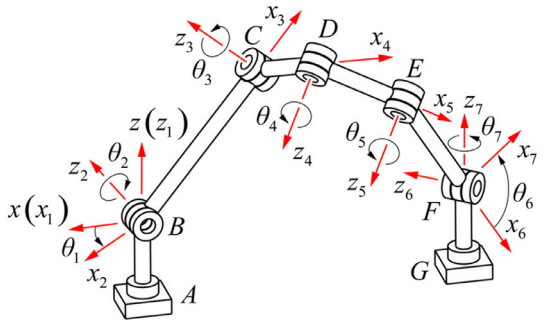

Fig. 6. Another Schatz-inspired metamorphic mechanism.

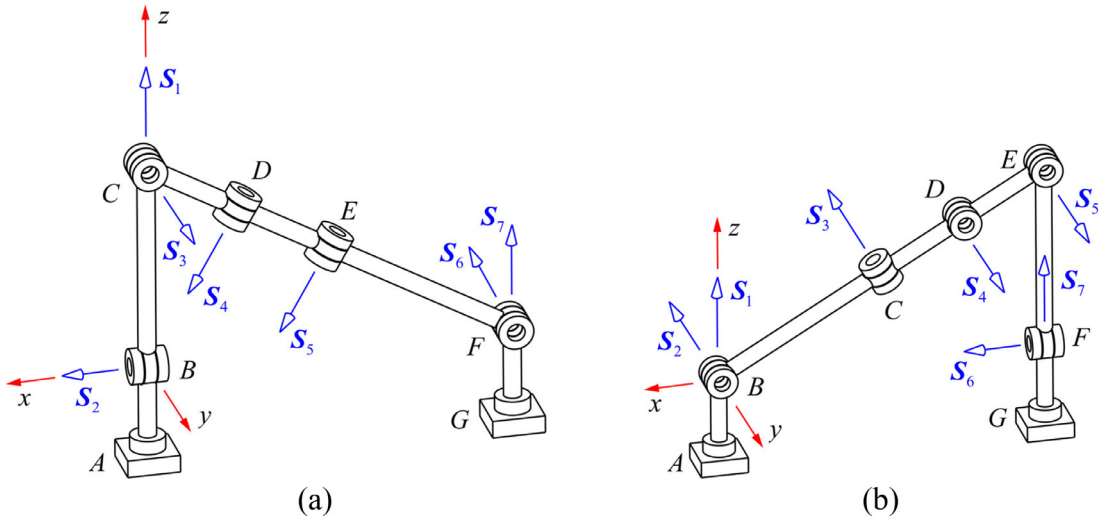

Fig. 7. Singular configuration I (a) and singular configuration II (b) of another Schatz-inspired metamorphic mechanism.

Seven screws that are attached to the seven revolute joints at the singular configuration I in Fig. 7(a) can be calculated and written as

$$\begin{aligned}
&\boldsymbol{S}_1 = (0,0,1,0,0,0)^{\mathrm{T}}, \boldsymbol{S}_2 = (1,0,0,0,0,0)^{\mathrm{T}}\\
&\boldsymbol{S}_3 = (0,1,0,-2,0,0)^{\mathrm{T}}, \boldsymbol{S}_4 = \left(\tfrac{1}{2},0,-\tfrac{\sqrt{3}}{2},0,0,0\right)^{\mathrm{T}}\\
&\boldsymbol{S}_5 = \left(\tfrac{1}{2},0,-\tfrac{\sqrt{3}}{2},0,-1,0\right)^{\mathrm{T}}, \boldsymbol{S}_6 = \left(0,-1,0,0,0,2\sqrt{3}\right)^{\mathrm{T}}\\
&\boldsymbol{S}_7 = \left(0,0,1,0,2\sqrt{3},0\right)^{\mathrm{T}}
\end{aligned} \tag{44}$$

Similarly, the seven screws at the singular configuration II in Fig. 7(b) can also be calculated and written as

$$\begin{aligned}
&\boldsymbol{S}_1 = (0,0,1,0,0,0)^{\mathrm{T}}, \boldsymbol{S}_2 = (0,-1,0,0,0,0)^{\mathrm{T}}\\
&\boldsymbol{S}_3 = \left(\tfrac{1}{2},0,\tfrac{\sqrt{3}}{2},0,2,0\right)^{\mathrm{T}}, \boldsymbol{S}_4 = \left(0,1,0,-\tfrac{3}{2},0,-\tfrac{3\sqrt{3}}{2}\right)^{\mathrm{T}}\\
&\boldsymbol{S}_5 = \left(0,1,0,-2,0,-2\sqrt{3}\right)^{\mathrm{T}}, \boldsymbol{S}_6 = (1,0,0,0,0,0)^{\mathrm{T}}\\
&\boldsymbol{S}_7 = \left(0,0,1,0,2\sqrt{3},0\right)^{\mathrm{T}}
\end{aligned} \tag{45}$$

Substituting the seven screws of Eq. (44) into Eq. (5), the Jacobian matrix of singular configuration I in Fig. 7(a) and the first-order velocity constraint equations at singular configuration I are obtained as

$$\boldsymbol{J\omega} = \begin{bmatrix}
0 & 1 & 0 & \frac{1}{2} & \frac{1}{2} & 0 & 0\\
0 & 0 & 1 & 0 & 0 & -1 & 0\\
1 & 0 & 0 & -\frac{\sqrt{3}}{2} & -\frac{\sqrt{3}}{2} & 0 & 1\\
0 & 0 & -2 & 0 & 0 & 0 & 0\\
0 & 0 & 0 & 0 & -1 & 0 & 2\sqrt{3}\\
0 & 0 & 0 & 0 & 0 & 2\sqrt{3} & 0
\end{bmatrix}\begin{bmatrix}
\omega_1\\ \omega_2\\ \omega_3\\ \omega_4\\ \omega_5\\ \omega_6\\ \omega_7
\end{bmatrix} = \mathbf{0} \tag{46}$$

It can be found that the second, fourth and sixth rows of the Jacobian matrix in Eq. (46) are dependent.

Substituting the seven screws of Eq. (44) into Eq. (9), the Lie screw $\boldsymbol{S}_L$ can be obtained and simplified as

$$\boldsymbol{S}_L = \begin{pmatrix}
0\\ \frac{\sqrt{3}}{2}\omega_2\left(\omega_4+\omega_5\right)\\ 0\\ 2\omega_5\omega_7\\ 0\\ \sqrt{3}\omega_5\omega_7
\end{pmatrix} \tag{47}$$

The algebraic condition for solving Eq. (13) is that all the six-order cofactors of the extended matrix $[\boldsymbol{J}\ -\boldsymbol{S}_L]$ are zero. Thus, the second-order velocity constraint equations can be obtained by calculating all the six-order cofactors of the augmented matrix as

$$\sqrt{3}\omega_5\omega_7 + \omega_2\omega_4 + \omega_2\omega_5 = 0 \tag{48}$$

Assembling the first-order velocity constraint equations in Eq. (46) and the second-order velocity constraint equations in Eq. (48), the following constraint system with first- and second-order velocity constraints integrated is obtained and all possible constraints exerted to the mechanism at singular configuration I can be listed as

$$\begin{cases}
\omega_2 + \frac{1}{2}\omega_4 + \frac{1}{2}\omega_5 = 0\\
\omega_1 - \frac{\sqrt{3}}{2}\omega_4 - \frac{\sqrt{3}}{2}\omega_5 + \omega_7 = 0\\
\omega_3 = 0\\
-\omega_5 + 2\sqrt{3}\omega_7 = 0\\
\omega_6 = 0\\
\sqrt{3}\omega_5\omega_7 + \omega_2\omega_4 + \omega_2\omega_5 = 0
\end{cases} \tag{49}$$

Then, two linearly independent solutions are obtained. If representing these solutions in the form of 7-dimensional column vectors $(\omega_1\ \omega_2\ \ldots\ \omega_7)^{\mathrm{T}}$, the solution vectors can be expressed as

$$\left(2\omega_7 \quad -\sqrt{3}\omega_7 \quad 0 \quad 0 \quad 2\sqrt{3}\omega_7 \quad 0 \quad \omega_7\right)^{\mathrm{T}} \tag{50}$$

$$\left(-4\omega_7 \quad \sqrt{3}\omega_7 \quad 0 \quad -4\sqrt{3}\omega_7 \quad 2\sqrt{3}\omega_7 \quad 0 \quad \omega_7\right)^{\mathrm{T}} \tag{51}$$

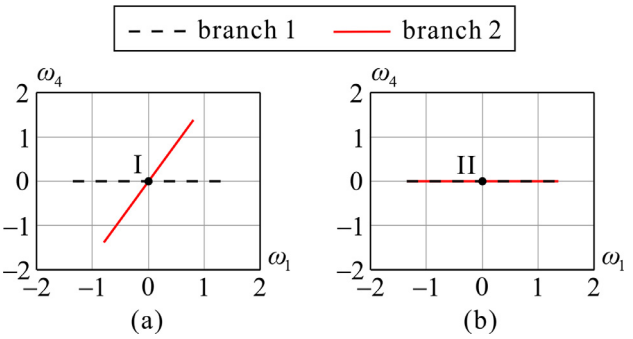

Fig. 8. The relation of angular velocities$\omega_4$vs$\omega_1$at singular configuration I (a) and singular configuration II (b).

Similar to singular configuration I in Fig. 7(a), substituting the seven screws of Eq. (45) into Eq. (5), first-order velocity constraint equations at singular configuration II in Fig. 7(b) are obtained as

$$\boldsymbol{J}\omega = \begin{bmatrix} 0 & 0 & \frac{1}{2} & 0 & 0 & 1 & 0 \\ 0 & -1 & 0 & 1 & 1 & 0 & 0 \\ 1 & 0 & \frac{\sqrt{3}}{2} & 0 & 0 & 0 & 1 \\ 0 & 0 & 0 & -\frac{3}{2} & -2 & 0 & 0 \\ 0 & 0 & 2 & 0 & 0 & 0 & 2\sqrt{3} \\ 0 & 0 & 0 & -\frac{3\sqrt{3}}{2} & -2\sqrt{3} & 0 & 0 \end{bmatrix} \begin{bmatrix} \omega_1 \\ \omega_2 \\ \omega_3 \\ \omega_4 \\ \omega_5 \\ \omega_6 \\ \omega_7 \end{bmatrix} = \mathbf{0} \tag{52}$$

Substituting the seven screws of Eq. (45) into Eq. (9), the Lie screw $\boldsymbol{S}_L$ of singular configuration II can be expressed and simplified as

$$\boldsymbol{S}_L = \begin{pmatrix} -\sqrt{3}\omega_2\omega_3 \\ \frac{\sqrt{3}}{2}\omega_3\omega_6 \\ \omega_2\omega_3 \\ -\omega_3\omega_7 - \frac{\sqrt{3}}{2}\omega_4\omega_5 \\ 0 \\ \frac{1}{2}\omega_4\omega_5 - 2\omega_3\omega_6 \end{pmatrix} \tag{53}$$

Thus, the second-order velocity constraint equations of the Schatz-inspired metamorphic mechanism at singular configuration II in Fig. 7(b) can be obtained by calculating all the six-order cofactors of the augmented matrix as

$$\omega_4\omega_5 - \omega_3\omega_6 + \frac{\sqrt{3}}{2}\omega_3\omega_7 = 0 \tag{54}$$

Then, the following constraint system with first and second-order kinematics is obtained as

$$\begin{cases} \frac{1}{2}\omega_3 + \omega_6 = 0 \\ -\omega_2 + \omega_4 + \omega_5 = 0 \\ \omega_1 + \frac{\sqrt{3}}{2}\omega_3 + \omega_7 = 0 \\ -\frac{3}{2}\omega_4 - 2\omega_5 = 0 \\ 2\omega_3 + 2\sqrt{3}\omega_7 = 0 \\ \omega_4\omega_5 - \omega_3\omega_6 + \frac{\sqrt{3}}{2}\omega_3\omega_7 = 0 \end{cases} \tag{55}$$

Only one linearly independent solution is obtained. If representing it in a 7-dimensional column vector $(\omega_1\ \omega_2\ \omega_3\ \omega_4\ \omega_5\ \omega_6\ \omega_7)^{\mathrm{T}}$, the solution vector can be expressed as

$$\left(\frac{1}{2}\omega_7 \quad 0 \quad -\sqrt{3}\omega_7 \quad 0 \quad 0 \quad \frac{\sqrt{3}}{2}\omega_7 \quad \omega_7\right)^{\mathrm{T}} \tag{56}$$

Comparing Eqs. (50)(51) and Eq. (56), it can be found that there are two linearly independent solutions, which means there are two different motion branches that can be revealed through the first- and second-order based method at singular configuration I in Fig. 7(a). However, there is only one linearly independent solution and it cannot be revealed whether there are different motion branches at singular configuration II in Fig. 7(b), of which the reason is that the two motion branches have the same velocity at singular configuration II as shown in Fig. 8(b). In other words, the kinematic curves of these two motion branches are tangent at singular configuration II. Meanwhile, as shown in Fig. 8(a), the two motion branches have different velocities at singular configuration I and the kinematic curves of these two motion branches intersect at singular configuration II. In a word, the first- and second-order based method succeeds in the revelation of different motion branches at singular configuration I but fails to reveal different motion branches at singular configuration II. Then, it needs to calculate the acceleration relation of kinematic joints at singular configuration II in the following section.

Substituting Eqs. (45), (53) and (56) into Eq. (13), the second-order acceleration constraint equations at singular configuration II can be written as

$$\boldsymbol{J\alpha}=\begin{bmatrix} 0 & 0 & \frac{1}{2} & 0 & 0 & 1 & 0\\ 0 & -1 & 0 & 1 & 1 & 0 & 0\\ 1 & 0 & \frac{\sqrt{3}}{2} & 0 & 0 & 0 & 1\\ 0 & 0 & 0 & -\frac{3}{2} & -2 & 0 & 0\\ 0 & 0 & 2 & 0 & 0 & 0 & 2\sqrt{3}\\ 0 & 0 & 0 & -\frac{3\sqrt{3}}{2} & -2\sqrt{3} & 0 & 0 \end{bmatrix}\begin{bmatrix} \alpha_1\\ \alpha_2\\ \alpha_3\\ \alpha_4\\ \alpha_5\\ \alpha_6\\ \alpha_7 \end{bmatrix}=\begin{pmatrix} 0\\ \frac{3\sqrt{3}}{4}\omega_7^2\\ 0\\ -\sqrt{3}\omega_7^2\\ 0\\ -3\omega_7^2 \end{pmatrix} \tag{57}$$

Then, we need to calculate the third-order kinematics to obtain other acceleration constraint equations. The jerk screw $\boldsymbol{S}_J$ can be written as

$$\boldsymbol{S}_J=\begin{bmatrix} \left(\frac{3}{2}\alpha_2+3\alpha_4+3\alpha_5\right)\omega_7-\frac{9\sqrt{3}}{8}\omega_7^3\\ \left(\frac{3}{4}\alpha_3-3\alpha_6\right)\omega_7\\ -\frac{3\sqrt{3}}{2}(\alpha_4+\alpha_5)\omega_7+\frac{9}{8}\omega_7^3\\ -3\alpha_3\omega_7\\ -\left(\frac{9}{4}\alpha_4+3\alpha_5\right)\omega_7+\sqrt{3}\omega_7^3\\ 6\sqrt{3}\alpha_6\omega_7 \end{bmatrix} \tag{58}$$

The algebraic condition for solving Eq. (29) is that all the six-order cofactors of the extended matrix $[\boldsymbol{J}\ -\boldsymbol{S}_J]$ are zero. Thus, the third-order acceleration constraint equations can be obtained by calculating all the six-order cofactors of the extended matrix as

$$\omega_7(\alpha_3+2\alpha_6)=0 \tag{59}$$

Comparing Eq. (59) and the first second-order acceleration constraint equation in Eq. (57), we can find that these two equations are equivalent to each other, which means that the third-order acceleration constraint equation cannot be used for the revelation of bifurcation. Further, we need to calculate the fourth-order kinematics to attain other acceleration constraint equations as follows.

Then, the jounce screw $\boldsymbol{S}_{J0}$ can be written as

$$\boldsymbol{S}_{J0}=\begin{bmatrix} (2\rho_2+4\rho_4+4\rho_5)\omega_7+\frac{9}{4}\alpha_4\alpha_7-\frac{9\sqrt{3}}{2}\alpha_7\omega_7^2\\ (\rho_3-4\rho_6)\omega_7-\frac{9\sqrt{3}}{4}\alpha_7^2-\frac{9}{4}\alpha_4\omega_7^2-\frac{27\sqrt{3}}{8}\omega_7^4\\ -2\sqrt{3}(\rho_4+\rho_5)\omega_7-\frac{3\sqrt{3}}{4}\alpha_4\alpha_7+\frac{9}{4}\alpha_7\omega_7^2\\ -4\rho_3\omega_7+\frac{9\sqrt{3}}{8}\alpha_4^2+3\sqrt{3}\alpha_7^2+\frac{9}{2}\alpha_4\omega_7^2+\frac{9+36\sqrt{3}}{8}\omega_7^4\\ -(3\rho_4+4\rho_5)\omega_7+3\sqrt{3}\alpha_4\omega_7^2\\ 8\sqrt{3}\rho_6\omega_7-\frac{9}{8}\alpha_4^2+9\alpha_7^2+\frac{9\sqrt{3}}{2}\alpha_4\omega_7^2+\frac{27}{2}\omega_7^4 \end{bmatrix} \tag{60}$$

The algebraic condition for solving Eq. (35) is that all the six-order cofactors of the extended matrix $[\boldsymbol{J}\ -\boldsymbol{S}_{J0}]$ are zero. Thus, the fourth-order acceleration constraint equations can be obtained by calculating all the six-order cofactors of the extended matrix and simplified as

$$\alpha_4\left(\alpha_4+2\sqrt{3}\omega_7^2\right)=0 \tag{61}$$

Assembling Eqs. (57) and (61), all possible acceleration constraints at the singular configuration II can be listed as

$$\begin{cases} \frac{1}{2}\alpha_3+\alpha_6=0\\ -\alpha_2+\alpha_4+\alpha_5=\frac{3\sqrt{3}}{4}\omega_7^2\\ \alpha_1+\frac{\sqrt{3}}{2}\alpha_3+\alpha_7=0\\ -\frac{3}{2}\alpha_4-2\alpha_5=-\sqrt{3}\omega_7^2\\ 2\alpha_3+2\sqrt{3}\alpha_7=0\\ \alpha_4\left(\alpha_4+2\sqrt{3}\omega_7^2\right)=0 \end{cases} \tag{62}$$

Two linearly independent solutions are obtained. If representing these solutions in the form of 7-dimensional column vectors $(\alpha_1\ \alpha_2\ \ldots\ \alpha_7)^{\mathrm{T}}$, the solution vectors can be expressed as

$$\left(\frac{1}{2}\alpha_7\quad -\frac{\sqrt{3}}{4}\omega_7^2\quad -\sqrt{3}\alpha_7\quad 0\quad \frac{\sqrt{3}}{2}\omega_7^2\quad \frac{\sqrt{3}}{2}\alpha_7\quad \alpha_7\right)^{\mathrm{T}} \tag{63}$$

$$\left(\frac{1}{2}\alpha_7\quad -\frac{3\sqrt{3}}{4}\omega_7^2\quad -\sqrt{3}\alpha_7\quad -2\sqrt{3}\omega_7^2\quad 2\sqrt{3}\omega_7^2\quad \frac{\sqrt{3}}{2}\alpha_7\quad \alpha_7\right)^{\mathrm{T}} \tag{64}$$

These two linearly independent solutions correspond to two different motion branches revealed by the third- and fourth-order based method. Considering these two relations of joint angular accelerations in Eqs. (63) and (64) as shown in Fig. 9

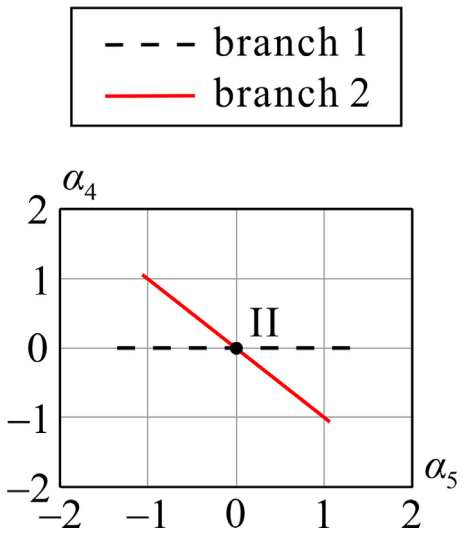

Fig. 9. The relation of angular accelerations$\alpha_4$vs$\alpha_5$at singular configuration II.

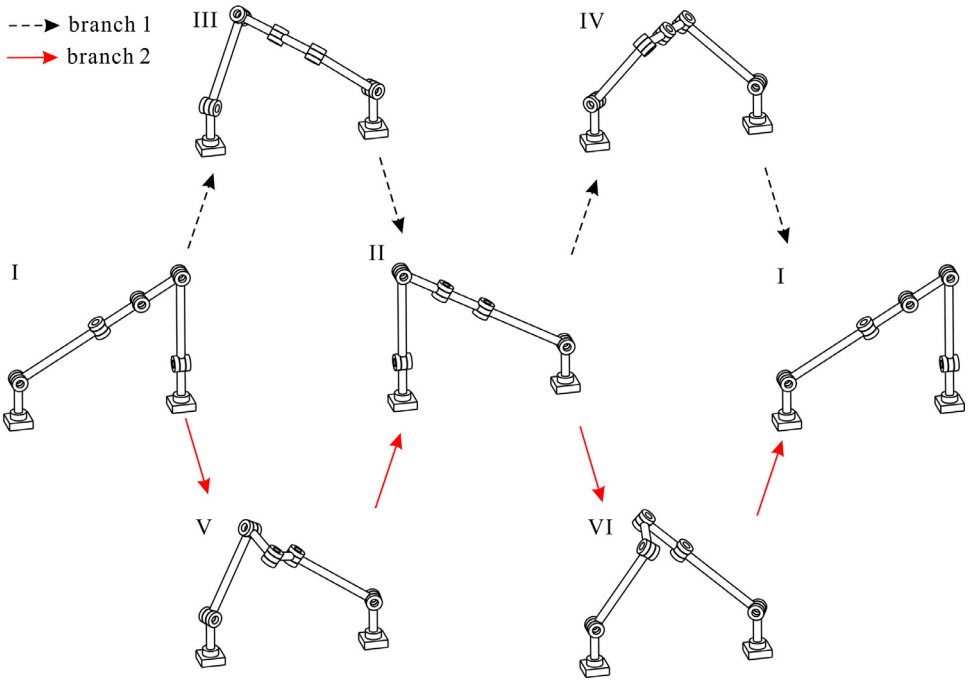

Fig. 10. Motion branches of another Schatz-inspired metamorphic mechanism.

with the relation of joint angular velocity in Eq. (56) at singular configuration II, the difference between these two motion branches is that revolute joint D is geometrically constrained in one motion branch while not geometrically constrained in the other motion branch. In other words, when the mechanism moves through singular configuration II in Fig. 7(b), the curvatures of kinematic curves of these two motion branches are different, although the tangent lines of them are the same.

When the angles between the axis of joint D and those of joints C and E are both $\pi/4$ as shown in [51], the mechanism has four motion branches and twelve bifurcation points, which can be revealed by the first- and second-order based method. However, when the angle between the axis of joint D and those of joints C and E are $\pi/2$ and 0, respectively, as presented in Fig. 6, the mechanism has two motion branches and two bifurcation points, where bifurcation point I can be revealed by the first- and second-order based method while bifurcation point II can only be revealed by the third- and fourth-order based method rather than the first- and second-order based method as shown in Figs. 8 and 9.

All the motion branches and singular configurations in the mechanism as shown in Fig. 10, where I-III-II-IV-I correspond to configurations of the mechanism along motion branch 1 and I-V-II-VI-I correspond to configurations of the mechanism along motion branch 2.

The mechanism moves as a Schatz mechanism along motion branch 1 and as a single degree-of-freedom spatial mechanism along motion branch 2, where joint D is geometrically constrained in motion branch 1 but not in motion branch 2. When the mechanism moves to singular configurations, the mechanism will be divided into two motion branches and this is coined as bifurcation. The mechanism can switch its motion branches when going through the intersection points and these points can thus be coined as constraint singularity. It can realise the reconfigurable switch between these two motion branches through singular configuration I and singular configuration II.

7. Conclusions

This paper established the high-order kinematic models of the Schatz-inspired metamorphic mechanisms and obtained velocity constraint equations and acceleration constraint equations using the sequential operation of the Lie bracket. Based on these velocity constraint equations, bifurcation of the presented mechanism at singular configuration I was revealed by the first- and second-order based method, but those at singular configuration II was not. The reason was that there was only one linearly independent relationship between joint angular velocities, which means the motion branches had the same velocity at singular configuration II and kinematic curves of these motion branches were tangent. Further, we proposed a novel third- and fourth-order based method to reveal it.

Based on the simplified higher-order kinematic model, we calculated the acceleration constraint equations from the second-, third- and fourth-order kinematics, in which the third-order acceleration constraint equations were equivalent to those of second-order and cannot be used for the revelation of bifurcation. Then, two linearly independent relationships between joint angular accelerations were attained and the bifurcation characteristics at singular configuration II were revealed with these acceleration constraint equations, which correspond to different curvatures of kinematic curves of the two motion branches, although the tangent lines of them were the same. It would be found that the first- and second-order based method was based on the tangent change of motion branches, while the third- and fourth-order based method was based on the curvature change of motion branches.

In a similar way, we can discover other novel metamorphic mechanisms induced by classical overconstrained mechanisms except the Schatz mechanism, which may have a similar phenomenon. Moreover, when the motion branches of these mechanisms have the same tangential velocity at the singular configuration, the higher-order kinematics than second-order is needed. Hence, this research provided a more general procedure for revealing motion branches of reconfigurable mechanisms, which is to use the first- and second-order based method firstly followed by the third- and fourth-order based method if there exists the same velocity at the singular configuration.

Declaration of Competing Interests

None.

Acknowledgement

This work was supported in part by Singapore A*STAR SERC (Grant No. 1922500054), in part by the Natural Science Foundation of China (Grant No. 51535008) and by NSFC innovation research group project on equipment mechanism theory and technical foundation (Grant no. 51721003) and in part by the Engineering and Physical Sciences Research Council (EPSRC) of UK (Grant No. EP/P026087/1, EP/S019790/1).

Appendix

The detailed items of the jerk screw $\boldsymbol{S}_J$ are

$$2\sum_{i<j}\omega_i\alpha_j\left[\boldsymbol{S}_i,\boldsymbol{S}_j\right]=\begin{pmatrix}-(4\alpha_3+2\alpha_5+2\alpha_6)\omega_7\\(4\alpha_2-\alpha_4)\omega_7\\-2\sqrt{3}\alpha_3\omega_7\\4\alpha_4\omega_7\\-(8\alpha_3+\alpha_5)\omega_7\\2\sqrt{3}\alpha_4\omega_7\end{pmatrix}\quad\sum_{i<j}\alpha_i\omega_j\left[\boldsymbol{S}_i,\boldsymbol{S}_j\right]=\begin{pmatrix}-(2\alpha_3+\alpha_5+\alpha_6)\omega_7\\\left(2\alpha_2-\frac{1}{2}\alpha_4\right)\omega_7\\-\sqrt{3}\alpha_3\omega_7\\2\alpha_4\omega_7\\-\left(4\alpha_3+\frac{1}{2}\alpha_5\right)\omega_7\\\sqrt{3}\alpha_4\omega_7\end{pmatrix}$$

$$\sum_{i<j}\omega_i\omega_i\omega_j\left[\boldsymbol{S}_i,\left[\boldsymbol{S}_i,\boldsymbol{S}_j\right]\right]=\begin{pmatrix}-3\sqrt{3}\omega_7^3\\0\\3\omega_7^3\\0\\-18\sqrt{3}\omega_7^3\\0\end{pmatrix}\quad 2\sum_{i<j<k}\omega_i\omega_j\omega_k\left[\boldsymbol{S}_i,\left[\boldsymbol{S}_j,\boldsymbol{S}_k\right]\right]=\begin{pmatrix}12\sqrt{3}\omega_7^3\\0\\6\omega_7^3\\0\\28\sqrt{3}\omega_7^3\\0\end{pmatrix}$$

The detailed items of the jounce screw $\boldsymbol{S}_{J0}$ are

$$3\sum_{i<j}\omega_i\rho_j\left[\boldsymbol{S}_i,\boldsymbol{S}_j\right]=\begin{pmatrix}-(6\rho_3+3\rho_5+3\rho_6)\omega_7\\ \left(6\rho_2-\frac{3}{2}\rho_4\right)\omega_7\\ -3\sqrt{3}\rho_3\omega_7\\ 6\rho_4\omega_7\\ -\left(12\rho_3+\frac{3}{2}\rho_5\right)\omega_7\\ 3\sqrt{3}\rho_4\omega_7\end{pmatrix}\quad\sum_{i<j}\rho_i\omega_j\left[\boldsymbol{S}_i,\boldsymbol{S}_j\right]=\begin{pmatrix}-(2\rho_3+\rho_5+\rho_6)\omega_7\\ \left(2\rho_2-\frac{1}{2}\rho_4\right)\omega_7\\ -\sqrt{3}\rho_3\omega_7\\ 2\rho_4\omega_7\\ -\left(4\rho_3+\frac{1}{2}\rho_5\right)\omega_7\\ \sqrt{3}\rho_4\omega_7\end{pmatrix}$$

$$3\sum_{i<j}\alpha_i\alpha_j\left[\boldsymbol{S}_i,\boldsymbol{S}_j\right]=\begin{pmatrix}6\alpha_2\left(-3\omega_7^2+\sqrt{3}\alpha_3\right)\\ -3\sqrt{3}\alpha_2^2\\ 6\alpha_2\alpha_3\\ 4\sqrt{3}\alpha_2^2+18\sqrt{3}\alpha_3^2-216\alpha_3\omega_7^2+180\sqrt{3}\omega_7^4\\ 12\alpha_2\left(-2\omega_7^2+\sqrt{3}\alpha_3\right)\\ 6\alpha_2^2+18\alpha_3^2-72\sqrt{3}\alpha_3\omega_7^2+180\omega_7^4\end{pmatrix}$$

$$3\sum_{i<j}\omega_i\omega_i\alpha_j\left[\boldsymbol{S}_i,\left[\boldsymbol{S}_i,\boldsymbol{S}_j\right]\right]=\begin{pmatrix}9\alpha_2\omega_7^2\\ \omega_7^2\left(-171\sqrt{3}\omega_7^2+36\alpha_3\right)\\ -3\sqrt{3}\alpha_2\omega_7^2\\ -\omega_7^2\left(-156\sqrt{3}\omega_7^2+36\alpha_3\right)\\ 54\alpha_2\omega_7^2\\ -\omega_7^2\left(-378\omega_7^2+36\sqrt{3}\alpha_3\right)\end{pmatrix}\quad3\sum_{i<j}\omega_i\alpha_i\omega_j\left[\boldsymbol{S}_i,\left[\boldsymbol{S}_i,\boldsymbol{S}_j\right]\right]=\begin{pmatrix}9\alpha_2\omega_7^2\\ 0\\ -3\sqrt{3}\alpha_2\omega_7^2\\ 0\\ 54\alpha_2\omega_7^2\\ 0\end{pmatrix}$$

$$6\sum_{i<j<k}\omega_i\omega_j\alpha_k\left[\boldsymbol{S}_i,\left[\boldsymbol{S}_j,\boldsymbol{S}_k\right]\right]=\begin{pmatrix}-36\alpha_2\omega_7^2\\ -\omega_7^2\left(-162\sqrt{3}\omega_7^2+54\alpha_3\right)\\ -6\sqrt{3}\alpha_2\omega_7^2\\ \omega_7^2\left(-144\sqrt{3}\omega_7^2+72\alpha_3\right)\\ -84\alpha_2\omega_7^2\\ \omega_7^2\left(-324\omega_7^2+36\sqrt{3}\alpha_3\right)\end{pmatrix}$$

$$3\sum_{i<j<k}\omega_i\alpha_j\omega_k\left[\boldsymbol{S}_i,\left[\boldsymbol{S}_j,\boldsymbol{S}_k\right]\right]=\begin{pmatrix}-18\alpha_2\omega_7^2\\ -\omega_7^2\left(9\sqrt{3}\omega_7^2+18\alpha_3\right)\\ -3\sqrt{3}\alpha_2\omega_7^2\\ \omega_7^2\left(12\sqrt{3}\omega_7^2+18\alpha_3\right)\\ -42\alpha_2\omega_7^2\\ \omega_7^2\left(54\omega_7^2+6\sqrt{3}\alpha_3\right)\end{pmatrix}\quad3\sum_{i<j<k}\alpha_i\omega_j\omega_k\left[\boldsymbol{S}_i,\left[\boldsymbol{S}_j,\boldsymbol{S}_k\right]\right]=\begin{pmatrix}-18\alpha_2\omega_7^2\\ 0\\ -3\sqrt{3}\alpha_2\omega_7^2\\ 18\alpha_3\omega_7^2\\ -42\alpha_2\omega_7^2\\ -6\sqrt{3}\alpha_3\omega_7^2\end{pmatrix}$$

$$\sum_{i<j}\omega_i\omega_i\omega_i\omega_j\left[\boldsymbol{S}_i,\left[\boldsymbol{S}_i,\left[\boldsymbol{S}_i,\boldsymbol{S}_j\right]\right]\right]=\begin{pmatrix}0\\ 18\sqrt{3}\omega_7^4\\ 0\\ -48\sqrt{3}\omega_7^4\\ 0\\ -72\omega_7^4\end{pmatrix}\quad3\sum_{i<j<k}\omega_i\omega_i\omega_j\omega_k\left[\boldsymbol{S}_i,\left[\boldsymbol{S}_i,\left[\boldsymbol{S}_j,\boldsymbol{S}_k\right]\right]\right]=\begin{pmatrix}0\\ 45\sqrt{3}\omega_7^4\\ 0\\ -48\sqrt{3}\omega_7^4\\ 0\\ -54\omega_7^4\end{pmatrix}$$

$$3\sum_{i<j<k}\omega_i\omega_j\omega_j\omega_k\left[\boldsymbol{S}_i,\left[\boldsymbol{S}_j,\left[\boldsymbol{S}_j,\boldsymbol{S}_k\right]\right]\right]=\begin{pmatrix}0\\ -27\sqrt{3}\omega_7^4\\ 0\\ 108\sqrt{3}\omega_7^4\\ 0\\ 162\omega_7^4\end{pmatrix}$$

$$6\sum_{h<i<j<k}\omega_h\omega_i\omega_j\omega_k\left[\boldsymbol{S}_h,\left[\boldsymbol{S}_i,\left[\boldsymbol{S}_j,\boldsymbol{S}_k\right]\right]\right]=\begin{pmatrix}0\\ 0\\ 0\\ -72\sqrt{3}\omega_7^4\\ 0\\ 0\end{pmatrix}$$

References

[1] K. Wohlhart, Kinematotropic linkages, Recent Adv. Robot Kinemat. (1996) 359–368.
[2] J.S. Dai, J. Rees Jones, Mobility in metamorphic mechanisms of foldable/erectable kinds, ASME J. Mech. Des. 121 (3) (1999) 375–382.
[3] D. Gan, J.S. Dai, Geometry constraint and branch motion evolution of 3-PUP parallel mechanisms with bifurcated motion, Mech. Mach. Theory 61 (2013) 168–183.
[4] Y. Qin, J.S. Dai, G. Gogu, Multi-furcation in a derivative queer-square mechanism, Mech. Mach. Theory 81 (2014) 36–53.
[5] H. Feng, Y. Chen, J.S. Dai, G. Gogu, Kinematic study of the general plane-symmetric Bricard linkage and its bifurcation variations, Mech. Mach. Theory 116 (2017) 89–104.
[6] H. Feng, J. Ma, Y. Chen, Z. You, Twist of tubular mechanical metamaterials based on waterbomb origami, Sci. Rep. 8 (1) (2018) 1–13.
[7] X. Ma, X. Zhang, J.S. Dai, Motion cycle and configuration torus with their relationship to furcation during reconfiguration, ASME J. Mech. Robot. 10 (5) (2018) 051006.
[8] Y. Song, X. Ma, J.S. Dai, A novel 6R metamorphic mechanism with eight motion branches and multiple furcation points, Mech. Mach. Theory 142 (2019) 103598.
[9] P. Kumar, S. Pellegrino, Computation of kinematic paths and bifurcation points, Int. J. Solids Struct. 37 (46-47) (2000) 7003–7027.
[10] W.W. Gan, S. Pellegrino, Numerical approach to the kinematic analysis of deployable structures forming a closed loop, IMechE J. Mech. Eng. Sci. 220 (7) (2006) 1045–1056.
[11] J.S. Dai, Z. Huang, H. Lipkin, Mobility of overconstrained parallel mechanisms, ASME J. Mech. Des. 128 (1) (2006) 220–229.
[12] X. Kang, J.S. Dai, Relevance and transferability for parallel mechanisms with reconfigurable platforms, J. Mech. Robot. 11 (3) (2019) 031012.
[13] D. Gan, J.S. Dai, J. Dias, L. Seneviratne, Unified kinematics and singularity analysis of a metamorphic parallel mechanism with bifurcated motion, J. Mech. Robot. 5 (3) (2013) 031004.
[14] D. Gan, J.S. Dai, Q. Liao, Constraint analysis on mobility change of a novel metamorphic parallel mechanism, Mech. Mach. Theory 45 (12) (2010) 1864–1876.
[15] C. Gao, H. Huang, B. Li, G. Jia, Design of a truss-shaped deployable grasping mechanism using mobility bifurcation, Mech. Mach. Theory 139 (2019) 346–358.
[16] J. Wei, J.S. Dai, Reconfiguration-aimed and manifold-operation based type synthesis of metamorphic parallel mechanisms with motion between 1R2T and 2R1T, Mech. Mach. Theory 139 (2019) 66–80.
[17] J. Wei, J.S. Dai, Lie group based type synthesis using transformation configuration space for reconfigurable parallel mechanisms with bifurcation between spherical motion and planar motion, J. Mech. Des. 142 (6) (2020) 063302.
[18] Y.X. Wang, Y.M. Wang, Configuration bifurcations analysis of six degree-of-freedom symmetrical stewart parallel mechanisms, ASME J. Mech. Des. 127 (1) (2005) 70–77.
[19] C.C. Lee, J.M. Herve, A novel discontinuously movable six-revolute mechanism, in: 2009 ASME/IFToMM International Conference on Reconfigurable Mechanisms and Robots, KC Edizioni, London, 2009, pp. 58–62.
[20] Q. Li, J.M. Herve, Parallel mechanisms with bifurcation of Schoenflies motion, IEEE Trans. Robot. 25 (1) (2009) 158–164.
[21] G. Gogu, Bifurcation in constraint singularities and structural parameters of parallel mechanisms, Meccanica 46 (1) (2011) 65–74.
[22] X.F. Yuan, L. Zhou, Y.F. Duan, Singularity and kinematic bifurcation analysis of pin-bar mechanisms using analogous stiffness method, Int. J. Solids Struct. 49 (10) (2012) 1212–1226.
[23] L. Nurahmi, S. Caro, P. Wenger, J. Schadlbauer, M. Husty, Reconfiguration analysis of a 4-RUU parallel manipulator, Mech. Mach. Theory 96 (2016) 269–289.
[24] K.H. Hunt, Kinematic Geometry of Mechanisms, Oxford University Press, Oxford, 1978.
[25] J.P. Merlet, Jacobian, manipulability, condition number and accuracy of parallel robots, ASME J. Mech. Des. 128 (128) (2006) 199–206.
[26] F. Tahmasebi, L.W. Tsai, Jacobian and stiffness analysis of a novel class of six-DOF parallel minimanipulators, ASME Des. Eng. Division 47 (1992) 95–102.
[27] J. Wang, C.M. Gosselin, Kinematic analysis and singularity representation of spatial five-degree-of-freedom parallel mechanisms, J. Robot. Syst. 14 (12) (1997) 851–869.
[28] T. Huang, M. Li, X. Zhao, J. Mei, D.G. Chetwynd, S.J. Hu, Conceptual design and dimensional synthesis for a 3-DOF module of the TriVariant-a novel 5-DOF reconfigurable hybrid robot, IEEE Trans. Robot. 21 (3) (2005) 449–456.
[29] L.W. Tsai, Solving the inverse dynamics of a Stewart-Gough manipulator by the principle of virtual work, ASME J. Mech. Des. 122 (1) (2000) 3–9.
[30] W. Khalil, S. Guegan, Inverse and direct dynamic modeling of Gough-Stewart robots, IEEE Trans. Robot. 20 (4) (2004) 754–761.
[31] M. Callegari, M.-C. Palpacelli, M. Principi, Dynamics modelling and control of the 3-RCC translational platform, Mechatronics 16 (10) (2006) 589–605.
[32] T. Sun, S. Yang, B. Lian, Finite and Instantaneous Screw Theory in Robotic Mechanism, Springer, Singapore, 2020.
[33] T. Sun, S. Yang, An approach to formulate the Hessian matrix for dynamic control of parallel robots, IEEE/ASME Trans. Mechatron. 24 (1) (2019) 271–281.
[34] T. Sun, S. Yang, T. Huang, J.S. Dai, A finite and instantaneous screw based approach for topology design and kinematic analysis of 5-axis parallel kinematic machines, Chin. J. Mech. Eng. 31 (1) (2018). 44(10 pages).
[35] T. Sun, S. Yang, T. Huang, J.S. Dai, A way of relating instantaneous and finite screws based on the screw triangle product, Mech. Mach. Theory 108 (2017) 75–82.
[36] S.A. Joshi, L.W. Tsai, Jacobian analysis of limited-DOF parallel manipulators, ASME J. Mech. Des. 124 (2) (2002) 254–258.
[37] M. Thomas, D. Tesar, Dynamic modeling of serial manipulator arms, J. Dyn. Syst., Meas., Control 104 (3) (1982) 218–228.
[38] H. Wang, Z. Huang, Kinematic influence coefficient method of kinematic and dynamic analysis, Mech. Mach. Theory 25 (2) (1990) 167–173.
[39] S. Staicu, D. Zhang, A novel dynamic modelling approach for parallel mechanisms analysis, Rob. Comput. Integr. Manuf. 24 (1) (2008) 167–172.
[40] S. Staicu, Inverse dynamics of the 3-PRR planar parallel robot, Robot. Auton. Syst. 57 (5) (2009) 556–563.
[41] J.M. Rico, J. Duffy, An application of screw algebra to the acceleration analysis of serial chains, Mech. Mach. Theory 31 (4) (1996) 445–457.
[42] J.M. Rico, J. Gallardo, J. Duffy, Screw theory and higher order kinematic analysis of open serial and closed chains, Mech. Mach. Theory 34 (4) (1999) 559–586.
[43] J.G. Alvarado, Análisis Cinemáticos de Orden Superior de Cadenas Espaciales, Mediante el Algebra de Tornillos, y sus Aplicaciones, Instituto tecnológico de la Laguna, 1999.
[44] J. Gallardo-Alvarado, M.A. Garcia-Murillo, Rigid body hyper-jerk analysis using screw theory, in: Multibody Mechatronic Systems, Springer, 2015, pp. 411–422.
[45] P.C. López-Custodio, J.M. Rico, J.J. Cervantes-Sánchez, G.I. Pérez-Soto, C.R. Díez-Martínez, Verification of the higher order kinematic analyses equations, Eur. J. Mech. A/Solids 61 (2017) 198–215.
[46] J. Lerbet, Analytic geometry and singularities of mechanisms, Z. Angew. Math. Mech. 78 (10) (1998) 687–694.
[47] X. Kang, X. Zhang, J.S. Dai, First-and second-order kinematics-based constraint system analysis and reconfiguration identification for the queer-square mechanism, ASME J. Mech. Robot. 11 (1) (2019) 011004.
[48] R.S. Hartenberg, J. Denavit, Kinematic Synthesis of Linkages, McGraw-Hill, 1964.
[49] R.M. Murray, Z. Li, S.S. Sastry, A Mathematical Introduction to Robotic Manipulation, CRC Press, 1994.
[50] G. Strang, Linear Algebra and its Applications, Academic Press Inc, New York, 1976.
[51] X. Kang, X. Ma, J.S. Dai, H. Yu, Bifurcation variations and motion-ruled-surface evolution of a novel Schatz linkage induced metamorphic mechanism, Mech. Mach. Theory 150 (2020) 103867.